Constraining short-range spin-dependent forces with polarized He 3

M. Guigue, D. Jullien, A. k. Petukhov, G. Pignol

PHYSICAL REVIEW D **92,** 114001 (2015)

Constraining short-range spin-dependent forces with polarized ^{3}He

M. Guigue,[1,*] D. Jullien,[2] A. K. Petukhov,[2] and G. Pignol[1,†]
[1]*LPSC, Université Grenoble-Alpes, CNRS/IN2P3, Grenoble, France*
[2]*Institut Laue Langevin, 53, Rue Horowitz 38000, Grenoble*
(Received 3 September 2015; published 1 December 2015)

We have searched for a short-range spin-dependent interaction using the spin relaxation of hyperpolarized ^{3}He. Such a new interaction would be mediated by a hypothetical light scalar boson with *CP*-violating couplings to the neutron. The walls of the ^{3}He cell would generate a pseudomagnetic field and induce an extra depolarization channel. We did not see any anomalous spin relaxation, and we report the limit for interaction ranges λ between 1 and 100 μm, $g_s g_p \lambda^2 \leq 2.6 \times 10^{-28}$ m^2 (95% C.L.), where $g_s(g_p)$ are the (pseudo)scalar coupling constant, improving the previous best limit by 1 order of magnitude.

DOI: 10.1103/PhysRevD.92.114001 PACS numbers: 67.30.ep, 11.30.Er, 13.75.Cs

I. INTRODUCTION

Theories beyond the Standard Model (SM) of particle physics generically predict the existence of new particles. They can broadly be divided into two categories, *ultraviolet* and *infrared* modifications of the SM.

Concerning the ultraviolet category, new particles are expected with masses above the electroweak scale of about 100 GeV. For example, grand unified theories are associated with an energy scale as high as 10^{15} GeV. In the case of supersymmetry and similar theories, new particles could be discovered just above the electroweak scale. These particles are still actively searched for in high energy proton-proton collisions at the Large Hadron Collider. Although it is perhaps too early to reach a definitive conclusion, as a matter of fact, no evidence for the existence of new physics in the TeV range has been reported by Run 1 of the LHC.

Alternatively, new physics could manifest itself in the infrared, that is, at energies much below the electroweak scale (see Ref. [1] for a review on the low energy frontier of particle physics). In this case, one should look for weakly interacting slim particles (WISPs), having masses below 1 eV.

Nambu–Goldstone scalar bosons, arising from the spontaneous breaking of a global symmetry, establish a well-motivated theoretical case for WISPs. These bosons are naturally predicted to be very light, even massless if the symmetry is not explicitly broken. The prominent example is the hypothetical QCD axion, the boson associated with the global $U(1)$ Peccei–Quinn symmetry introduced to solve the strong *CP* problem [2]. The QCD axion is basically a one-parameter theory: its mass and couplings to SM particles can be derived from a single symmetry breaking scale parameter f_a, which lies presumably between 10^9 and 10^{12} GeV. One can imagine other Nambu–Goldstone bosons with no specific relation between the mass, symmetry breaking scale and the couplings to SM particles, these bosons being referred to as axionlike particles or ALPs. It is interesting to note that, although ALPs induce new phenomena in the infrared (because they are very light), they are associated with a symmetry breaking at an energy scale well above the electroweak scale, as is the case for the QCD axion. Other than spin-0 ALPs, there can exist new light spin-1 bosons, arising from broken hidden $U(1)$ symmetries, which do no decouple from SM particles even in the limit of vanishing mass [3].

The existence of dark matter provides another motivation to search for new light particles, since it turns out that WISPs are suitable dark matter candidates [4,5]. Experiments aiming at detecting WISPy dark matter, called *haloscopes*, are very different from detectors searching for weakly interacting massive particles. Instead of catching hits of single particles, one needs to detect an oscillating field. For example, ADMX [6] uses a resonant cavity to convert these oscillations to microwave photons, provided the WISP couples with the photon.

Regardless of the WISPs being the dark matter, astrophysical objects like the Sun or supernovae could be a sizable source of WISPs via thermal production. A too big escape channel for WISPs would contradict the observed time scale of the evolution of stars. This "energy loss" argument provides stringent bounds on the coupling of WISPs with SM particles [7]. Experiments such as CAST [8] aim at detecting the flux of WISPs emitted by the Sun, by converting them into x-ray photons in a so-called *helioscope*.

It is desirable to design laboratory experiments to search for WISPs that do not rely on a cosmological or astrophysical source. Only the combination of independent results can confirm or discard the existence of exotic bosons. One type of laboratory experiments is *light shining through a wall* (see Ref. [9] for a review) probing the

*guigue@lpsc.in2p3.fr
†pignol@lpsc.in2p3.fr

WISP-photon coupling. Another type of experiments, to probe the couplings to fermions, consists of searching for a *fifth force*. The exchange of an exotic light boson between two fermions induces a macroscopic force which is derived from a Yukawa potential [10],

$$V(x) = \frac{g_s^2}{4\pi}\frac{\hbar c}{x}\mathrm{e}^{-x/\lambda}, \tag{1}$$

with g_s the coupling constants of the boson to the fermions at the interaction vertex and x the distance between the two fermions. The interaction range λ is given by

$$\lambda = \frac{\hbar c}{m_0 c^2}, \tag{2}$$

with m_0 the mass of the light boson. While the range of the interaction induced by a heavy boson like the W ($m_W = 80$ GeV) is as short as 10^{-15} m, a boson lighter than 0.1 eV will generate macroscopic effects between objects separated by 2 μm. Numerous experiments searching for this fifth force have been realized for a wide range of boson masses (see Ref. [11] for a review of this topic).

The potential (1) corresponds to the most simple version with a scalar coupling g_s to a fermion, resulting in a monopole-monopole interaction. Now, in the presence of a pseudoscalar coupling $ig_p\gamma^5$, the interaction becomes *spin dependent* and cannot be discovered by fifth force experiments using macroscopic bodies. In this paper, we report on a search for a spin-dependent interaction of the type

$$V(x) = g_s g_p \frac{n\lambda\hbar^2}{4m}\sigma_z e^{-x/\lambda}, \tag{3}$$

generated by a macroscopic source of unpolarized nucleons with volumic density n acting on a polarized probe with spin σ_z and mass m. The nucleons occupy an infinite thick plate, and the probe is situated outside of the plate at a distance x from the surface. The constant g_s is the scalar coupling of the source nucleon to the boson, and g_p is the pseudoscalar coupling constant between the probe and the boson. The potential (3) corresponds to the sum of two monopole-dipole potentials $\mathcal{V}_{9,10}$ presented in Dobrescu and Mocioiu 's classification [12].

As a practical realization, we considered a ^{3}He polarized gas contained in a glass cell. The source of the interaction acting on the ^{3}He spins is the nucleons in the walls of the cell. The helium spins then probe a short-range pseudomagnetic field,

$$b(x) = g_s g_p \frac{\lambda\hbar}{2m\gamma} e^{-x/\lambda}, \tag{4}$$

with $\gamma/2\pi = 32.4$ Hz/μT [13] the gyromagnetic ratio of the ^{3}He atoms. The motion of the spins in this pseudomagnetic field will induce an anomalous longitudinal depolarization of the gas, in addition to the usual depolarization mechanisms. By studying the longitudinal relaxation rate of the ^{3}He gas as a function of the applied magnetic field, this effect can be separated from the other standard contributions.

In the case of the QCD axion, when taking into account the bound on the QCD CP-violating phase $\theta < 10^{-10}$ derived from the most recent measurement of the neutron electric dipole moment (nEDM) [14], the product of the coupling constants $g_s g_p$ is predicted to be typically smaller than 10^{-26} for a 1 μm range [10], which is more than 10 orders of magnitude below the current sensitivity. However, in the generic case of ALPs, no such prediction exists.

In 2010, a preliminary experiment [15] performed at the Institut Laue-Langevin (ILL) measured the depolarization rate of a hyperpolarized ^{3}He gas and set a competitive constraint on the $g_s g_p$ coupling. To improve our sensitivity, we built a dedicated setup at the ILL. The enhancement of sensitivity, as compared to other techniques, comes from the very long relaxation time (several days under certain conditions) of the polarized gas.

In Sec. II, we will review the theory of depolarization of particles moving in an inhomogeneous field. The expression of the anomalous depolarization induced by the pseudomagnetic field will be also derived. The experimental apparatus will be presented in details in Sec. III. Finally, the results of data analysis and the obtained constraints will be shown in Sec. IV.

II. THEORY OF STANDARD AND EXOTIC SPIN RELAXATION OF ^{3}He

We consider the case of an assembly of spin-1/2 particles with a gyromagnetic ratio γ contained in a glass cell of volume V and immersed in a holding magnetic field $\vec{B}_0 = B_0\vec{e}_z$. The magnetic inhomogeneities are quantified by $\vec{b} = (b_x, b_y, b_z)$. The Larmor precession frequency of the spins is $\omega_0 = \gamma B_0$. The cell walls of thickness d act as a source of a pseudomagnetic field felt by a polarized particle,

$$\vec{b}_a(x) = b_a e^{-x/\lambda}\vec{e}_x, \tag{5}$$

orthogonal to the wall surface with $b_a = g_s g_p \frac{n\lambda\hbar}{2m\gamma}(1 - e^{-d/\lambda})$. The distance between the wall and the polarized particle is given by x. The density of nucleons in the glass (typically 1.6×10^{30} nucleons/m^3) is denoted n. The field components which are transverse to the holding field direction will induce a longitudinal relaxation of the particles polarization. The contribution to the relaxation induced by this short-range pseudomagnetic field (5) has a very peticular dependence on the holding magnetic field B_0: in certain conditions, the relaxation rate is proportional to $1/\sqrt{B_0}$, as we will show later on. In fact, the other depolarization channels one can expect behave as powers of $1/B_0$. In this section, we will discuss the expected

contributions to the depolarization. We will then use Redfield's theory of relaxation to calculate the relaxation rate associated with the magnetic inhomogeneities and by the sought short-range pseudomagnetic field.

A. Standard sources of relaxation

Since the ^{3}He gas polarization P is much larger than the polarization at the thermal equilibrium ($P(t=0) \approx 70\%$), the gas will depolarize as

$$P(t) = P(t=0)\exp(-\Gamma_1 t), \tag{6}$$

with Γ_1 the longitudinal relaxation rate. Three main phenomena contribute to the relaxation: collisions with the cell walls, collisions between ^{3}He atoms and particles motion in an inhomogeneous magnetic field. It is commonly known that the first contribution, quantified by Γ_w, does not depend on the gas polarization, its pressure and the holding field value [16,17]. The second contribution Γ_{dd} depends on the frequency of atomic collisions and thus is proportional to the pressure of the gas [18]. The last contribution is denoted Γ_m and corresponds to a perturbation of spins induced by their motion in an inhomogeneous magnetic field. Each atom effectively sees a fluctuating magnetic field, of which the transverse components fluctuations at the Larmor frequency induce spins inversions. This contribution has been discussed for decades in the literature. The calculation of the corresponding rate is presented in the next section.

B. Redfield theory and standard magnetic relaxation

To express the spin relaxation rate Γ_m of a polarized gas in slightly inhomogeneous magnetic fields, the Redfield theory [19] can be applied when the resulting relaxation time T_1 is much longer than the decay time of the magnetic field correlation functions. This condition is satisfied for a large variety of systems, such as a ^{3}He polarized gas at atmospheric pressure and immersed in a several μT holding field.

The relaxation rate of the gas can then be expressed as the Fourier transform of the transverse components correlation functions at the Larmor frequency of the spins,

$$\Gamma_m = \frac{1}{T_1} = \gamma^2 \int_0^\infty \langle b_x(0)b_x(\tau) + b_y(0)b_y(\tau)\rangle \cos(i\omega\tau)\mathrm{d}\tau. \tag{7}$$

The ensemble average (over the articles in the cell) is denoted $\langle\cdots\rangle$. The correlation function is the magnetic components b_i and b_j are expressed as

$$\langle b_i(0)b_j(\tau)\rangle = \frac{1}{V}\int_V \mathrm{d}\vec{r}_0 \int_V \mathrm{d}\vec{r} b_i(\vec{r}_0)b_j(\vec{r})\pi(\vec{r},\tau|\vec{r}_0). \tag{8}$$

The function $\pi(\vec{r},\tau|\vec{r}_0)$ corresponds to the conditional probability (also called the propagator) for a particle, being at $\tau = 0$ at $\vec{r}_0$, to be at τ at $\vec{r}$. In a general way, $\pi(\vec{r},\tau|\vec{r}_0)$ satisfies the initial condition

$$\pi(\vec{r},\tau=0|\vec{r}_0) = \delta(\vec{r}-\vec{r}_0) \tag{9}$$

and the boundary condition

$$\vec{\nabla}\pi(\vec{r},\tau|\vec{r}_0)\cdot\vec{n} = 0. \tag{10}$$

In the case of gases at several bars, the gas is in the "diffusive regime," and the propagator is governed by the diffusion equation

$$\frac{\partial\pi}{\partial\tau} = D\Delta\pi, \tag{11}$$

with D the diffusion coefficient of the gas. In the case of ^{3}He gas at a pressure of 1 bar, $D \approx 1.84\ \mathrm{cm}^2/\mathrm{s}$ [20,21].

For gases in the diffusive regime immersed in holding magnetic fields of several μT, there are several sources of magnetic inhomogeneities. For a given cell filled with a helium gas at a pressure p and a polarization P, the magnetic inhomogeneities are the sum of three terms:

$$\vec{b} = \vec{b}_{\mathrm{ext}} + \vec{b}_{\mathrm{coil}}(B_0) + \vec{b}_{\mathrm{cell}}(P,p). \tag{12}$$

The term $\vec{b}_{\mathrm{ext}}$ corresponds to magnetic inhomogeneities induced by the apparatus environment, and $\vec{b}_{\mathrm{coil}}(B_0)$ corresponds to the one created by the holding field generator and so is proportional to B_0. The last contribution $\vec{b}_{\mathrm{cell}}(P,p)$ is due to the fact that at high pressure and polarization the ^{3}He gas behaves as a magnet and generates an inhomogeneous magnetic field proportional to p and P.

For an arbitrary geometry cell immersed in a magnetic field with an arbitrary spatial profile, the relaxation rate can be estimated [22] with the relation

$$\Gamma_m = D\frac{\langle(\vec{\nabla}b_\perp)^2\rangle}{B_0^2}, \tag{13}$$

where $\langle(\vec{\nabla}b_\perp)^2\rangle$ corresponds to the average over the cell volume of the squared transverse gradients. Using (12), we can write the total longitudinal relaxation rate for a given pressure as

$$\Gamma_1 = a + \frac{b}{B_0} + \frac{c}{B_0^2} + \frac{dP}{B_0} + \frac{eP}{B_0^2} + \frac{fP^2}{B_0^2}, \tag{14}$$

with a, b, c, d, e and f real coefficients. For a given pressure in a given cell, the parameter a in (14) corresponds to the sum of the relaxation rates induced by atomic Γ_{dd} and walls Γ_w collisions, the spin-flip induced relaxation and the magnetic depolarization generated by the solenoid gradients. The third term c in (14) corresponds to the relaxation

induced by the environmental magnetic inhomogeneities $\vec{b}_{\text{ext}}$. The last term f in this equation corresponds to the depolarization induced by the field gradient generated by the polarized gas. The other coefficients b, d and e correspond to interference terms of magnetic gradients which have very different origins. For example, the coefficient b corresponds to the average value of the product of the solenoid magnetic gradients (which therefore depends on B_0) and the magnetic gradients induced by the environment (which does not depend on B_0). Coefficients a, c and f which have a clear physical meaning will be discussed in details in Sec. IV B.

C. Relaxation rate induced by a short-range spin-dependent interaction

If one assumes an exotic interaction (3) between the ^{3}He spins and the cell walls induced by a light boson, a new depolarization channel will be added to the standard relaxation (14). For simplicity, let us consider a one-dimensional problem: the source of the short-range pseudomagnetic field (5) is a glass plane of surface S and thickness d, placed in $x = 0$. The polarized particles evolve at the right side of the source for x positive. In this case, the constant b_a corresponds to the amplitude of the pseudomagnetic field (5) generated by the wall felt by the probe particle,

$$b_a = g_s g_p \frac{\hbar n \lambda}{2m\gamma}(1 - e^{-d/\lambda}), \tag{15}$$

with n the density of nucleons in the glass (typically 1.6×10^{30} nucleons/m^3). In the case of a polarized gas at atmospheric pressure and magnetic inhomogeneities larger than the mean free path of the probe particles, the diffusion equation (11) describes correctly the particle motion. The particle propagator can be expressed as a continuous sum of cosines,

$$\pi(\vec{r}, \tau|\vec{r}_0) = \frac{1}{S\pi}\int_{-\infty}^{\infty} dk \cos(kx)\cos(kx_0)\mathrm{e}^{-\tau D k^2}. \tag{16}$$

This expression assumes that the system is invariant under translations along $\vec{e}_y$ and $\vec{e}_z$. One can calculate the correlation function $\langle b(0)b(\tau)\rangle$ with b the pseudomagnetic component orthogonal to the surface,

$$\langle b(0)b(\tau)\rangle = \frac{b_a^2}{V\pi S} \times \int_{-\infty}^{\infty} \mathrm{d}k \left(\int_S \mathrm{d}y\mathrm{d}z \int_0^L \mathrm{d}x e^{-x/\lambda}\cos(kx)\right)^2 e^{-\tau D k^2}, \tag{17}$$

where L is defined as the ratio V/S. The length L corresponds to the characteristic distance between the walls of the cell. If the interaction range λ is much smaller than L, we can write

$$\langle b(0)b(\tau)\rangle = \frac{b_a^2 S}{V\pi}\int_{-\infty}^{\infty} \mathrm{d}k \left(\frac{\lambda}{1 + k^2\lambda^2}\right)^2 e^{-\tau D k^2}. \tag{18}$$

The relaxation rate (7) induced by a wall acting as a pseudomagnetic field source on a polarized particle is the Fourier transform of the correlation function (18) at the frequency ω_0,

$$\begin{aligned}\Gamma_{NF} &= \frac{\gamma^2}{2}\frac{b_a^2 S}{V\pi}\int_0^{\infty} \mathrm{d}\tau \cos(\omega_0\tau)\int_{-\infty}^{\infty} \mathrm{d}k \left(\frac{\lambda}{1 + k^2\lambda^2}\right)^2 e^{-\tau D k^2} \\ &= (\gamma b_a)^2 \frac{S}{V}\frac{\lambda^3}{2D}\frac{1}{(1 + \phi_\lambda^2)^2} \\ &\quad \times \left(\sqrt{\frac{2}{\phi_\lambda}}(1 - \phi_\lambda(\phi_\lambda - 2)) + \phi_\lambda^2 - 3\right),\end{aligned} \tag{19}$$

with $\phi_\lambda = \omega_0 \frac{\lambda^2}{D}$. The general solution of the one-dimension case of a polarized gas in the diffusive regime contained between two plates was treated in Ref. [15], using the Redfield theory and a propagator expansion with sines and cosines. Our result (19) is only valid in the limit $\omega_0 L^2/D \gg 1$.

In practice, polarized gases are contained in cubic, cylindrical or spherical cells with a wall thickness d. The longitudinal relaxation rate (19) can be adapted for any shape of cell with a typical size $L = V/S$, much larger than the interaction range λ. With this assumption, one can assume that the walls surface is flat: the relaxation rate induced by a short-range field for a cell is proportional to the calculated rate (19), valid for a flat surface. We can define the *apparent surface* S_a, corresponding to the cell surface which effectively contributes to the short-range relaxation

$$S_a = \int_S \mathrm{d}S[(\vec{e}_x \cdot \vec{n})^2 + (\vec{e}_y \cdot \vec{n})^2], \tag{20}$$

with $\vec{n}$ the unitary vector orthogonal to the surface. For example, the apparent surface of a sphere with radius R is $8\pi R^2/3$. Finally, the longitudinal relaxation rate of a polarized gas contained in a cell with a volume V and a typical size L larger than λ can be written, using the apparent surface S_a, as

$$\begin{aligned}\Gamma_{NF} &= (\gamma b_a)^2 \frac{S_a}{V}\frac{\lambda^3}{2D}\frac{1}{(1 + \phi_\lambda^2)^2} \\ &\quad \times \left(\sqrt{\frac{2}{\phi_\lambda}}(1 - \phi_\lambda(\phi_\lambda - 2)) + \phi_\lambda^2 - 3\right).\end{aligned} \tag{21}$$

In the case of a scalar-pseudoscalar interaction between a ^{3}He polarized gas and the nucleons in the cell walls, the relaxation rate is thus proportional to $(g_s g_p)^2$. Moreover, for $\phi_\lambda \ll 1 \ll \omega_0 L^2/D$, Eq. (22) simplifies into

$$\Gamma_{NF} = (\gamma b_a)^2 \frac{S_a}{2V} \sqrt{\frac{2\lambda^2}{D\omega_0}}, \tag{22}$$

which is valid for any shape of cell. In this regime, the behavior of the relaxation rate with respect to the holding field is very different from what could be expected (14). From Eq. (22) immediately follows that the behavior of the relaxations due to short-range forces in spherical and cubic cells are exactly the same since the factor S_a/V is equal to $2/R$ for a sphere with a radius R and $4/s$ for a cube with s the length of its edge.

The search of an exotic short-range interaction can be performed using polarized ^{3}He by measuring the relaxation of the gas as a function of the holding field and the polarization. If a deviation of the behavior of this rate is observed and corresponds to the induced short-range contribution (22), the existence of a new boson will be revealed.

III. EXPERIMENTAL SETUP AND PROCEDURE

The experimental method is rather straightforward in principle; it simply consists of measuring the relaxation rate of ^{3}He cells for different values of the holding magnetic field (and also for different values of the polarization of the cell). To polarize cells we have used the "Tyrex" Metastability Exchange Optical Pumping (MEOP) installation, described in details elsewhere [23]. The installation can provide up to 4 bars of polarized ^{3}He in a valved glass cell, at an initial polarization of up to 75%. The cell is then transferred to the apparatus dedicated to the measurement of the decay of the polarization, situated in the same building at the ILL. This apparatus is designed to operate a large range of possible holding magnetic fields B_0 ranging from 3 to 300 μT. In this section we present in detail the setup.

A. Magnetic environment

To decrease the magnetic depolarization contributions, the measurement of the gas polarization is performed in a very well-controlled magnetic environment. This apparatus is composed of a cylindrical mumetal magnetic shield and a solenoid.

A part of the mumetal tube, formerly used for the neutron-antineutron oscillations experiment at the ILL [24], was refurbished. This large tube [25] (1 m diameter, 4.5 m long and 0.8 mm thick) acts as a magnetic screen to shield the ambient magnetic field.

The 5 m long and 80 cm diameter solenoid is composed of 2363 spires around a 5 mm aluminum tube. It was installed inside the magnetic shield to provide a tunable, stable and homogeneous magnetic field in a large enough volume. Figure 1 shows the solenoid and the magnetic shield. For 1 A circulating current, the longitudinal magnetic field generated in the center of the solenoid is 590 μT.

FIG. 1 (color online). Solenoid inserted into the mumetal magnetic shield.

We performed several field maps (in a volume of $20 \times 20 \times 20$ cm^3) using a three-axis fluxgate magnetometer for various values of the holding field B_0. The maps were analyzed with a second-order 3D polynomial fit to extract the value of the transverse gradients $g_\perp$. The results are presented in Table I: typically, $g_\perp$ is about 2.4 to 4.2 nT/cm for a magnetic field from 2 to 80 μT. These weak magnetic gradients will give very long relaxation times T_1: a calculation from Eq. (13) gives times longer than 110 h for magnetic fields higher than 2 μT. Our magnetic apparatus can therefore be used to maintain ^{3}He cells polarized for several days.

B. Direct polarimetry

The spin relaxation rate is extracted by periodically measuring the polarization of a ^{3}He cell. We chose to use a direct polarimetry technique, first presented by Cohen Tannoudji [26]. It consists of recording the magnetic field generated by the magnetized cell itself, which is proportional to the polarization P. This is possible using commercial magnetometers since a fully polarized cell filled with 1 atm of ^{3}He generates a dipolar field of tens of nT.

Two Bartington low noise fluxgate magnetometers are placed where the dipolar field induced by the polarized gas is transverse relative to the B_0 field, as represented on Fig. 2. This configuration with two fluxgates allows one to

TABLE I. Results of the magnetic field mapping. The relaxation rates are calculated for a spherical 5 cm radius cell filled with 1 bar of ^{3}He.

B_0 (μT)	$\sqrt{g_\perp^2}$ (nT/cm)	$\Gamma_{1m,\text{calculated}}$ (h^{-1})
2.05	2.42	9.2×10^{-3}
10.47	2.47	3.7×10^{-4}
21.20	2.63	1.0×10^{-4}
83.81	4.21	1.7×10^{-5}

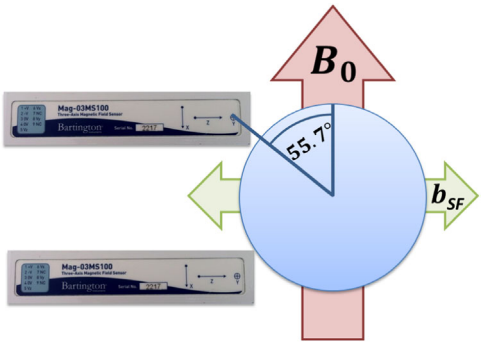

FIG. 2 (color online). Scheme of the spin-flipping and measurement apparatus. The spherical cell is positioned in contact with the two magnetometers inside the spin-flip coil which generates an oscillating magnetic field b_{SF} transversely to the holding magnetic field B_0.

compensate for the random fluctuations of the environmental transverse fields by taking the difference between the two magnetometer readings, as the dipolar fields created by the polarized ^{3}He gas at positions 1 and 2 are opposite. The performances of the setup in terms of the time stability are quantified by the Allan Standard Deviation shown in Fig. 3 for a holding field value of 80 μT: the difference reduces the long-time correlated fluctuations of the two fluxgates.

Applying spin flips with a transverse oscillating magnetic field to reverse the polarization, one can remove all magnetic contributions which are independent of the gas polarization, such as fluxgates offsets or a misalignment of the magnetometers' axes with B_0. This well-known technique, called "adiabatic fast passage" [27], requires a spin-flip coil and a RC circuit resonating at the Larmor frequency, corresponding to a 80 μT holding field.

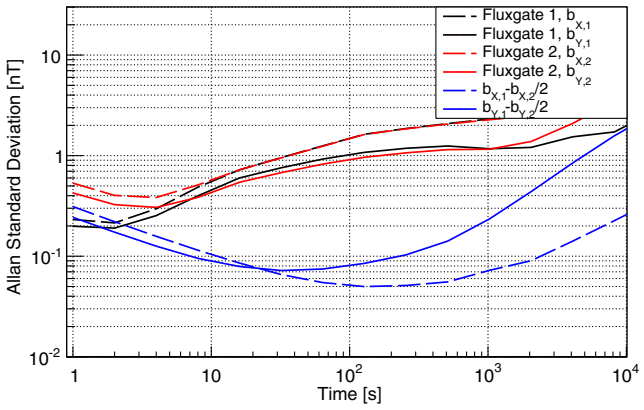

FIG. 3 (color online). Allan Standard Deviation (ASD) of the magnetic components transverse to the holding field direction for $B_0 = 80$ μT. The dashed lines correspond to the X component and the continuous lines to the Y component (X and Y are two directions orthogonal to B_0). In black, the ASD of fluxgate 1; in red, the ASD of fluxgate 2; in blue, the difference between the two fluxgates divided by 2.

An extension of this method to spin-flip polarized ^{3}He confined in a cell may be found in Ref. [28]. Our spin-flip coil is a solenoid of 50 cm long and 25 cm diameter with 50 turns of copper wires. Eleven additional turns at each end allow us to have a more homogeneous magnetic field in the spin-flip coil. The total resistance of the device is 21.8 Ohms. The spin-flip signal we used is an oscillating magnetic field b_{SF} directed orthogonally to the main field B_0. During the spin-flip signal, the frequency of this signal is swept through the Larmor frequency $f_0 = \gamma B_0/2\pi \approx 2.6$ kHz, and the signal envelop is modulated using a fourth-order polynomial shape,

$$B_1(t) = B_{1,\max}\left(\frac{2t}{\tau_{\mathrm{SF}}}\right)^2\left(2-\frac{2t}{\tau_{\mathrm{SF}}}\right)^2, \qquad (23)$$

with τ_{SF} the duration of the spin flip (in our case, $\tau_{\mathrm{SF}} = 100$ ms). The frequency-sweep range is equal to the spin Larmor frequency. This signal is generated by an NI-PCI6251 Multifunction Acquisition Card with an amplitude of 5.5 V. A voltage amplifier with a gain of 1.86 generates the oscillating current in the resonating circuit. To avoid maser effects which correspond to a strong coupling between the highly polarized gas and the spin-flip circuit [29], we used a rather low quality factor ($Q = 0.989$) and inserted in the resonating circuit a pair of diodes with low threshold (≈0.4 V) which decouples the spin-flip coil from the rest of the circuit between the spin-flip signals. Figure 4 presents a scheme of the spin-flip electronic device.

A polarization measurement sequence consists therefore of measuring the transverse magnetic field $b(\uparrow)$ with the two fluxgates during 1 s, applying a spin flip, measuring twice the magnetic field $b(\downarrow)$, applying a second spin flip and measuring the magnetic field $b(\uparrow)$ ($+--+$ *sequence*). Figure 5 shows typical sequences of $+--+$ measurements of the magnetic field induced by a spherical cell at 1 bar with the two magnetometers. The difference between the four measurements allows us to access directly to the magnetic field generated by the cell gas. Since this magnetic field is proportional to the gas polarization, one can deduce the polarization value at any time if given the

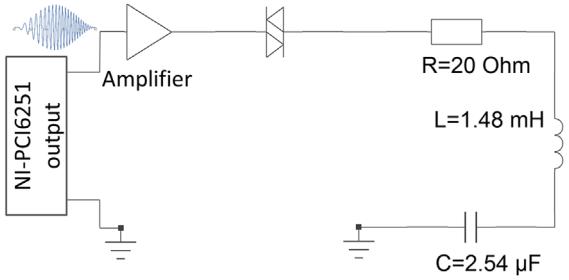

FIG. 4 (color online). Scheme of the spin-flip electronic device. It includes a NI-PCI6251 Multifunction Acquisition Card, an amplifier, a pair of diodes, a resistor, the spin-flip coil and a capacitor.

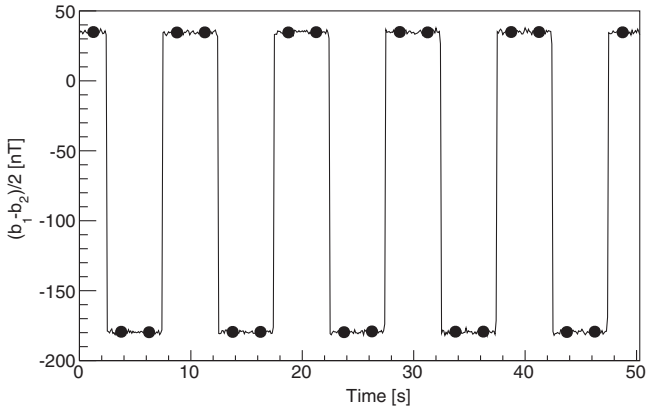

FIG. 5. Typical sequence of measurement of the transverse magnetic field generated by a cylindrical cell at 4 bars with two fluxgate magnetometers. The upper (lower) points correspond to the spin-up (-down) state of the gas.

initial polarization value. The polarization is expressed in nT; for example, a 5 cm radius spherical cell filled with 1 bar 70%-polarized gas cell generates a 30 nT magnetic field which is measured by the magnetometers at the glass surface. The statistical precision of one polarization measurement sequence, described above, is 0.16 nT. Repeating eight times this sequence will give a 60 pT precision and thus a signal to noise ratio of about 1000.

To determine the loss of polarization induced by a spin flip, we measured the loss of polarization induced by a large number of spin flips (about 10^4) during a short period (1 h). We conclude that each spin flip induces a loss of polarization of 3×10^{-6}. No dependence of these losses with the pressure or the polarization of the gas has been observed.

C. Structure of a measurement run

In the experiment, we measure the relaxation rate of spin-polarized ^{3}He gas as a function of the strength of the applied holding magnetic field B_0. In a given holding field value, the polarization measurement is done every 20 min. When the polarization relative loss is sufficient to precisely estimate the relaxation rate (≈10%), a new cycle begins, and the holding field value is changed. This procedure is repeated for holding fields between 3 and 90 μT: eight cycles correspond to a set of measurement. These sets are repeated until the polarization reaches a few nT. The combination of all the measured sets of one cell is called a *run*. The upper plot on Fig. 6 gives the result of Run 32 for a spherical cell, named "Axion01" of 6 cm radius filled with 1 bar of 70%-polarized ^{3}He. This cell possesses 3 mm thick aluminosilicate walls with a caesium coating and a cylindrical appendix, used to fill the cell with the helium gas. The typical relaxation time induced by the walls of this cell is about 400 h (see Sec. IV B 1). Because of this long T_1, a run using this cell lasts typically between 2 and 3 weeks. A smaller cell named CCT12 was also used for this experiment.

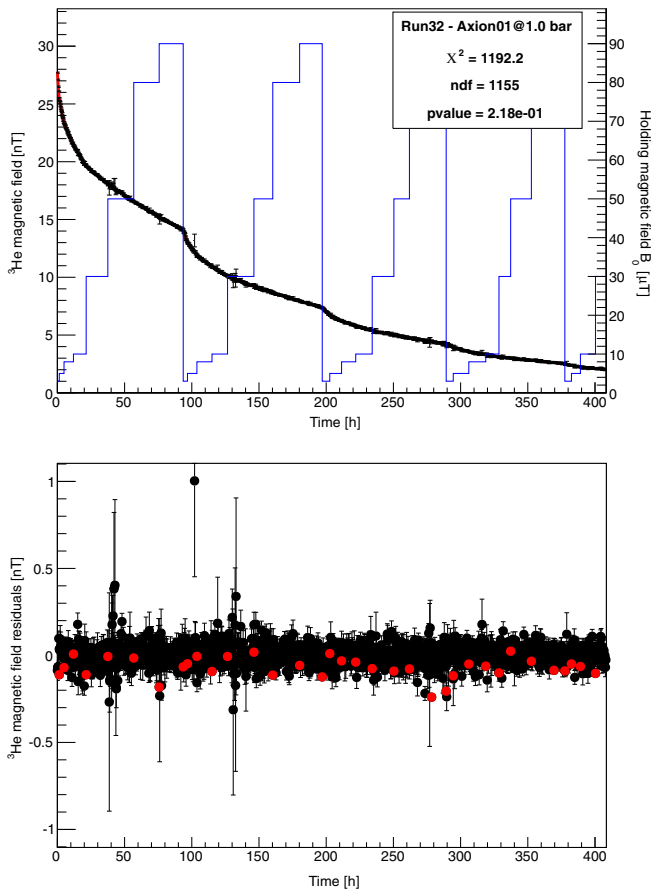

FIG. 6 (color online). Result of the χ^2 minimization method for Run 32. Up: the raw data (in black) and the best fit (in red) as a function of time and the holding field. The blue curve corresponds to the holding magnetic field value as a function of time. Down: residuals between the data and the polarization reconstruction. The red points correspond to the last measurement point of each T_1 measurement.

IV. ANALYSIS AND RESULTS

Runs have been performed for different spherical cells at different pressures. These characteristics are presented in Table II. For each run, the polarization as a function of time and holding field value is measured. Next, the gas relaxation is studied in order to find a deviation from the expected behavior (14).

In this section, the reconstruction method of the polarization as a function of time is presented. The extraction of the relaxation parameters for every run and the constraint on scalar-pseudoscalar coupling constants are then discussed in details.

A. Analysis procedure

At any time, for a given polarization value and magnetic field, the expected standard relaxation rate $\Gamma_1(P, B_0)$ is given by Eq. (14). If a new interaction between two nucleons mediated by a pseudoscalar boson exists, a

TABLE II. Main characteristics of the nine runs obtained with the apparatus. The value of the indicated initial polarization was measured on the Tyrex installation using an optical method [23].

Run	Cell	Radius (cm)	Pressure (bar)	Coating	Initial polarization
32	Axion01	6	1	Caesium	70%
33	Axion01	6	4	Caesium	70%
34	CCT12	4	4	Rubidium	70%
35	CCT12	4	1	Rubidium	70%
36	Axion01	6	2	Rubidium	70%
37	Axion01	6	3	Rubidium	70%
38	BufferAspec	6	1	None	70%
39	Axion01	6	0.3	Rubidium	70%
41	Axion01	6	3	Rubidium	70%

new depolarization channel (22) will add to the standard one. Therefore, the analysis procedure consists of reconstructing the polarization evolution as a function of time and holding field for a given boson mass or interaction range and compare it with the data. In the case of a polarization evolving slowly compared with the time between two polarization measurements, this step-by-step reconstruction is given by

$$P_{i+1}^{\mathrm{mod}} = P_i^{\mathrm{mod}} \exp\left(-\Gamma_1(P_i^{\mathrm{mod}}, B_i) \times (t_{i+1} - t_i)\right), \quad (24)$$

where P_i^{mod} denotes to the polarization at the time t_i.

First, only standard contributions to the relaxation rate (14) are taken into account. For a given set of parameters $\{a, \ldots, f, P_0\}$ with P_0 the initial polarization value (expressed in nT), the polarization reconstruction can be compared with the obtained measurements, using a χ^2 method. The minimization of such a quantity gives the most likely set of parameters. The result of this method is shown on Fig. 6. For each run, this reconstruction and analysis procedure is applied; plots analogue to Fig. 6 representing the raw data and the best fit are presented in the Supplemental Material [30]. Since the reduced χ^2 is close to 1, we can conclude no deviation in the data is observed; the standard contributions given by (14) explain the observed evolution of the polarization of each run.

B. Behavior of the fit parameters

For every run presented in Table II, we extracted the parameters of the standard depolarization (14) in the Axion01 cell for the different values of pressure. Among them, the parameters a, c and f have explicit physical meanings. Let us present their behavior with respect to the pressure.

1. Atomic and walls collisions depolarization

For a given pressure in a given cell, the a parameter in (14) corresponds to the sum of atomic Γ_{dd} and walls Γ_w collisions relaxations, the spin-flip induced relaxation and the magnetic depolarization generated by the solenoid gradients. The first contribution is proportional to the pressure. The depolarization induced by the spin flips (typically 6×10^{-6} h^{-1}) is independent of the gas polarization and the holding field value and contributes weakly to the parameter a compared with the atomic and walls collisions depolarization. The last contribution is inversely proportional to the pressure, but it is also expected to be very small compared with the two first ones.

Figure 7 presents the parameters a obtained in Runs 32, 33, 36, 37 and 39 as a function of the pressure in the Axion01 cell. A linear fit was performed in order to extract the relaxation times induced by the atomic and walls collisions. The measured atomic collisions relaxation time is 400 h for 1 bar of ^{3}He gas. A theoretical calculation of this contribution for gaseous ^{3}He predicts a lifetime of 798 h · bar [18]. This value does not correspond to the one extracted from our measurements. However, the presence of a few ppm of contaminants such as oxygen in the helium gas can explain this difference. Indeed, collisions between oxygen and helium can cause a new source of polarization relaxation with the same dependence on the pressure as He-He collisions depolarization.

Notice that the statistical error due to the measurement procedure is smaller than the point size on Fig. 7, while the data points present a significant spread. This can be understood taking into account that each measurement at a new pressure value required a new run of the Tyrex filling station to prepare a new filling with polarized gas. This complex procedure cannot guarantee the same T_1 due to the unavoidable contamination during the gas compression from mbar (the pressure at which the gas is optically polarized in Tyrex) to the desired pressure in a few bar range.

The walls induce a depolarization time of 460 h for the Axion01 cell. This long time is due to the high quality of the rubidium coating on the cell surface; an improvement of the walls quality by a factor of 2 will no longer make walls collisions relaxation a limiting contribution.

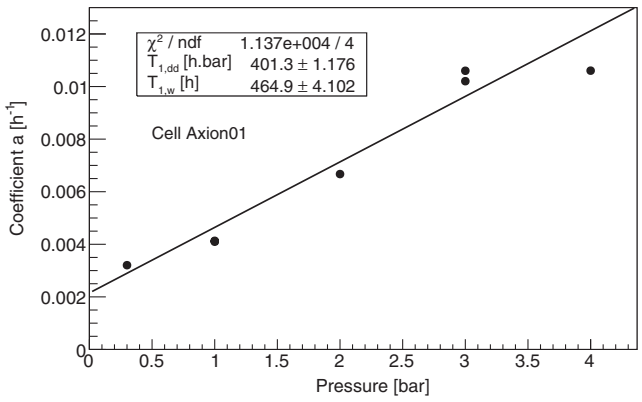

FIG. 7. Parameter a in (14) as a function of the pressure in the Axion01 cell.

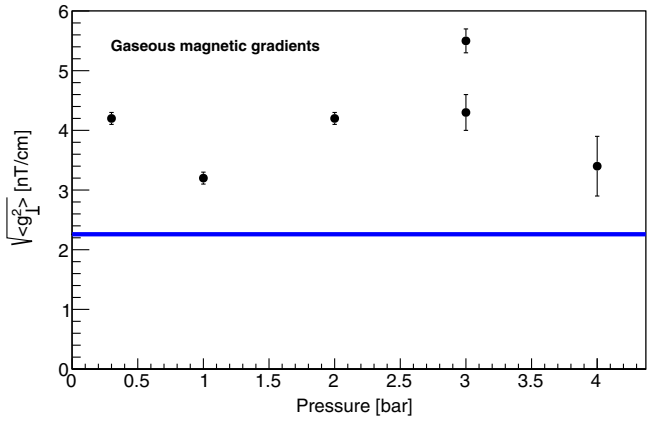

FIG. 8 (color online). Magnetic fields gradients extracted from the runs involving the Axion01 cell as a function of the pressure, corresponding to the parameter c in (14). The blue line corresponds to the gradient induced by the magnetic environment extracted from the magnetic maps.

2. Environment magnetic gradients depolarization

The third term c/B_0^2 in (14) corresponds to relaxation induced by the environmental magnetic inhomogeneities $\vec{b}_{\text{ext}}$. Figure 8 presents the transverse gradients $\sqrt{\langle g_\perp^2 \rangle}$ extracted from c using (13) as a function of the pressure for the Axion01 cell. The relative external magnetic gradients are typically smaller than 10^{-3} cm^{-1}, which corresponds to a relaxation time of 100 h at 3 μT. The difference of a few nT/cm between the mapping results presented in Table I and this gradients extraction is mainly due to the addition of material surrounding the cell, such as the spin-flip coil support.

3. Gaseous magnetic gradients depolarization

The relaxation rate (14) contains contributions which depend on the gas polarization P. The last term in this equation corresponds to the depolarization induced by the cell gradients. Figure 9 presents the equivalent transverse gradients $\sqrt{\langle g_\perp^2 \rangle}$ generated by a 100%-polarized gas using (13) as a function of the pressure in the cell. The magnetic gradients generated by 1 bar gas inside the Axion01 cell are about 13 nT/cm. These gradients limit the sensitivity of our experiment at a low magnetic field and high polarization. To improve the gradients generated by the gas polarization and improve the sensitivity of the method at high polarization, a dedicated study has been initiated.

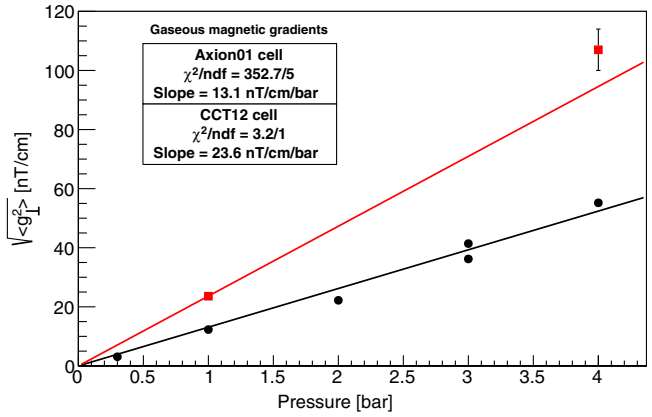

FIG. 9 (color online). Gaseous magnetic fields gradients extracted from the runs involving the Axion01 cell (black circles) and the CCT12 cell (red squares) as a function of the pressure, corresponding to the parameter f in (14).

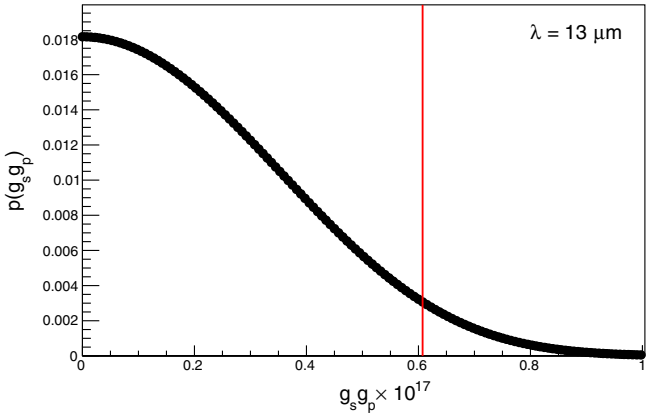

FIG. 10 (color online). *A posteriori* density function of the $g_s g_p$ parameter for $\lambda = 13$ μm obtained from Run 32. The integral to the left of the vertical red line corresponds to a 95% confidence level.

C. Extraction of constraints on a new interaction

To confirm the absence of a new short-range spin-dependent force which is derived from (3), a Bayesian approach is employed to extract the *a posteriori* probability density function of the parameters λ and $g_s g_p$. The relaxation rate induced by a short-range interaction is added to the standard depolarization contributions. The likelihood function $\mathcal{L}(\text{data}|a, \ldots, f, P_0, \lambda, g_s g_p)$ is built, assuming a Gaussian distribution of the data around the reconstruction model. Considering flat priors, the probability density

TABLE III. Constraints on $g_s g_p$ obtained with the nine runs. These constraints are valid for ranges between 1 and 100 μm.

Run	Cell	$g_s g_p \lambda$ (m^2) (95% C.L.)
32	Axion 01 @ 1 bar	11×10^{-28}
33	Axion 01 @ 4 bars	6.7×10^{-28}
34	CCT12 @ 4 bars	21×10^{-28}
35	CCT12 @1 bar	11×10^{-28}
36	Axion 01 @ 2 bars	11×10^{-28}
37	Axion 01 @ 3 bars	5.0×10^{-28}
38	BufferAspec @ 1 bar	60×10^{-28}
39	Axion 01 @ 0.3 bars	11×10^{-28}
41	Axion 01 @ 3 bars	4.4×10^{-28}

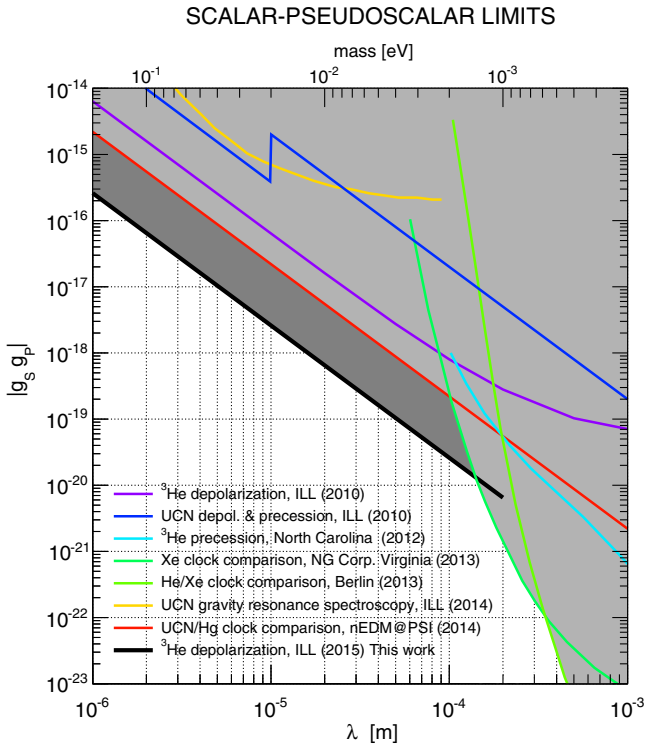

FIG. 11 (color online). Constraints on the coupling $g_s g_p$ of an interaction mediated by the exchange of a scalar boson as a function of the range λ and the mass given by $m_0 = \frac{\hbar}{\lambda c}$. Black: this work. Purple: ^{3}He relaxation rate measurements [15]. Dark blue: Ultra-Cold Neutrons (UCN) depolarization and precession [31]. Light blue: ^{3}He precession [32]. Light green: clock comparison with Xe isotopes [33]. Dark green: clock comparison with He and Xe [34]. Yellow: gravitational levels of UCN [35]. Red: Hg/UCN precession frequencies comparison [36].

function $p(\lambda, g_s g_p|\text{data})$ is obtained by marginalizing the likelihood function over the nuisance parameters $a, \ldots, f$ and P_0 and normalizing it to 1. For each range value λ between 1 and 100 μm, the *a posteriori* function is constructed as represented on Fig. 10. The maximum of this function is for $g_s g_p = 0$, which confirms that there is no evidence of a short-range interaction for the considered range of λ. To extract an upper limit on $g_s g_p$ for each λ with 95% C.L., an integration of the density function is performed. The upper limit $g_s g_{p,\text{lim}}$ is defined by

$$\int_0^{g_s g_{p,\text{lim}}} p(\lambda, g_s g_p|\text{data}) \mathrm{d} g_s g_p = 95\%. \tag{25}$$

Using Eq. (22) and the data obtained with Run 32, we put a constraint on the product $g_s g_p \lambda^2$ for ranges λ between 1 and 100 μm:

$$g_s g_p \lambda^2 \leq 1.1 \times 10^{-27}\ \text{m}^2 \quad (95\%\ \text{C.L.}). \tag{26}$$

For each run presented in Table II, this analysis procedure is applied, and no evidence of an exotic depolarization channel has been observed. Table III presents the constraints obtained on $g_s g_p \lambda^2$ for each run. A combination of these limits allows us to set a better constraint on the $g_s g_p$ product

$$g_s g_p \lambda^2 \leq 2.6 \times 10^{-28}\ \text{m}^2 \quad (95\%\ \text{C.L.}). \tag{27}$$

Figure 11 shows this constraint for ranges between 1 and 100 μm.

V. CONCLUSION

Measuring ^{3}He hyperpolarized gas relaxation as a function of the holding field is a sensitive method to search for short-range spin-dependent exotic interactions. To fully explore the potential of such a technique, a dedicated experimental setup was built with a particular effort on the reduction of magnetic inhomogeneities and the improvement of the polarization measurement. A more stringent constraint on the scalar-pseudoscalar coupling of an exotic boson to nucleons has been extracted from these measurements. Compared with the 2010 experiment [15], a factor 20 of improvement in terms of sensitivity has been obtained.

A significant improvement of more than 1 order of magnitude in sensitivity on $g_s g_p$ (corresponding to 2 orders of magnitude in terms of relaxation rate measurement) seems quite difficult to achieve, even in a better magnetic shield. Since our sensitivity is limited by the magnetic gradients generated by the polarized gas, significant efforts must be done in understanding the origin of the gas self-relaxation in order to overcome this limiting obstacle.

The obtained limit is better by a factor 8 than the previous best constraint obtained by the nEDM apparatus [36] and a factor 20 compared with the previous experiment performed in 2010 at ILL measuring ^{3}He longitudinal relaxation [15].

ACKNOWLEDGMENTS

We are thankful to Pierre Fayet, Pierre-Jean Nacher, and Geneviève Tastevin for fruitful discussions. We thank also the "Service Détecteurs et Instumentation" (SDI) from LPSC and Helium-3 group from ILL, especially Rémi Faure, Pascal Mouveau, and Antonello Rizo, for technical support. Part of this work was supported by the AGIR program of Université Joseph Fourier (Grenoble).

[1] J. Jaeckel and A. Ringwald, Annu. Rev. Nucl. Part. Sci. **60**, 405 (2010).
[2] J. E. Kim and G. Carosi, Rev. Mod. Phys. **82**, 557 (2010).
[3] P. Fayet, Nucl. Phys. **B347**, 743 (1990).
[4] A. Ringwald, Phys. Dark Univ. **1**, 116 (2012).
[5] P. Arias, D. Cadamuro, M. Goodsell, J. Jaeckel, J. Redondo, and A. Ringwald, J. Cosmol. Astropart. Phys. 06 (2012) 013.
[6] S. J. Asztalos *et al.*, Phys. Rev. Lett. **104**, 041301 (2010).
[7] G. G. Raffelt, *Stars as Laboratories for Fundamental Physics* (University of Chicago, Chicago, 1995).
[8] M. Arik *et al.*, Phys. Rev. Lett. **112**, 091302 (2014).
[9] J. Redondo and A. Ringwald, Contemp. Phys. **52**, 211 (2011).
[10] J. E. Moody and F. Wilczek, Phys. Rev. D **30**, 130 (1984).
[11] I. Antoniadis *et al.*, C.R. Phys. **12**, 755 (2011).
[12] B. A. Dobrescu and I. Mocioiu, J. High Energy Phys. 11 (2006) 005.
[13] J. L. Flowers, B. W. Petley, and M. G. Richards, Metrologia **30**, 75 (1993).
[14] J. M. Pendlebury *et al.*, Phys. Rev. D **92** (2015) 092003.
[15] A. K. Petukhov, G. Pignol, D. Jullien, and K. H. Andersen, Phys. Rev. Lett. **105**, 170401 (2010).
[16] R. E. Jacob, S. W. Morgan, B. Saam, and J. C. Leawoods, Phys. Rev. Lett. **87**, 143004 (2001).
[17] B. Saam, A. K. Petukhov, J. Chastagnier, T. R. Gentile, R. Golub, and C. M. Swank, Phys. Rev. A **85**, 047401 (2012).
[18] N. R. Newbury, A. S. Barton, G. D. Cates, W. Happer, and H. Middleton, Phys. Rev. A **48**, 4411 (1993).
[19] A. Redfield, Adv. Magn. Reson. **1**, 1 (1965).
[20] R. Barbé, M. Leduc, and F. Laloë, J. de Physique **35**, 935 (1974).
[21] M. E. Hayden, G. Archibald, K. M. Gilbert, and C. Lei, J. Magn. Reson. **169**, 313 (2004).
[22] M. Guigue, G. Pignol, R. Golub, and A. K. Petukhov, Phys. Rev. A **90**, 013407 (2014).
[23] K. H. Andersen, R. Chung, V. Guillard, H. Humblot, D. Jullien, E. Lelièvre-Berna, A. Petoukhov, and F. Tasset, Physica B (Amsterdam) **356**, 103 (2005).
[24] M. Baldo-Ceolin *et al.*, Z. Phys. C **63**, 409 (1994).
[25] T. Bitter, F. Eisert, P. El-Muzeini, M. Kessler, U. Kinkel, E. Klemt, W. Lippert, W. Meienburg, R. Werner, K. Gobrecht, and D. Dubbers, Nucl. Instrum. Methods Phys. Res., Sect. A **309**, 521 (1991).
[26] C. Cohen-Tannoudji, J. DuPont-Roc, S. Haroche, and F. Laloë, Phys. Rev. Lett. **22**, 758 (1969).
[27] V. Luschikov and Y. Taran, Nucl. Instrum. Methods Phys. Res., Sect. A **228**, 159 (1984).
[28] E. Babcock, A. Petoukhov, J. Chastagnier, D. Jullien, E. Lelièvre-Berna, K. Andersen, R. Georgii, S. Masalovich, S. Boag, C. Frost, and S. Parnell, Physica B (Amsterdam) **397**, 172 (2007).
[29] S. Bloom, J. Appl. Phys. **28**, 800 (1957).
[30] See Supplemental Material http://link.aps.org/supplemental/10.1103/PhysRevD.92.114001 for the complete data set and the associated fits.
[31] A. P. Serebrov, Phys. Lett. B **680**, 423 (2009).
[32] P.-H. Chu, A. Dennis, C. B. Fu, H. Gao, R. Khatiwada, G. Laskaris, K. Li, E. Smith, W. M. Snow, H. Yan, and W. Zheng, Phys. Rev. D **87**, 011105 (2013).
[33] M. Bulatowicz, R. Griffith, M. Larsen, J. Mirijanian, C. B. Fu, E. Smith, W. M. Snow, H. Yan, and T. G. Walker, Phys. Rev. Lett. **111**, 102001 (2013).
[34] K. Tullney *et al.*, Phys. Rev. Lett. **111**, 100801 (2013).
[35] T. Jenke *et al.*, Phys. Rev. Lett. **112**, 151105 (2014).
[36] S. Afach *et al.*, Phys. Lett. B **745**, 58 (2015).